Index Modulated OFDM Spread Spectrum

Qiang Li, Miaowen Wen, *Member, IEEE*, Ertugrul Basar, *Senior Member, IEEE*, and Fangjiong Chen, *Member, IEEE*

***Abstract*— In this paper, we propose an index modulated orthogonal frequency division multiplexing spread spectrum (IM-OFDM-SS) scheme, which combines the techniques of SS and IM under the framework of OFDM. In this scheme, the information bits are jointly conveyed by the indices of spreading codes and the conventional M-ary modulated symbols. A low-complexity maximal ratio combining (MRC) detector is designed, in which the receiver first detects the spreading codes and then de-spreads and demodulates the symbols. The bit error rate (BER) performance of IM-OFDM-SS systems in the presence of channel estimation errors is analyzed. An upper bound and approximate average bit error probability associated with maximum-likelihood and MRC detection, respectively, are derived. Subsequently, we extend the idea of IM-OFDM-SS to multi-code and multi-user scenarios, proposing generalized (G-)IM-OFDM-SS and IM-based multi-carrier code division multiple access (IM-MC-CDMA), respectively. Simulation results verify the analyses and show that the proposed IM/GIM-OFDM-SS outperforms the existing OFDM-IM and OFDM-SS schemes significantly. In addition, the IM-MC-CDMA exhibits a lower BER than MC-CDMA at the same SEs for either multi-user or single-user detection.**

***Index Terms*— OFDM, index modulation, spread spectrum, channel estimation errors, multi-user communications.**

I. Introduction

With the increasing demand for high data rate communications, multi-carrier transmission has received wide interest. The first orthogonal frequency division multiplexing (OFDM) scheme was proposed in 1966 [1], which presents the principle of orthogonal multiplexing for transmitting a number of information bits simultaneously without interchannel and intersymbol interferences. In [2], discrete Fourier transform (DFT) is used for baseband processing rather than a bank of oscillators, such that the implementation complexity of OFDM systems is greatly reduced. Furthermore, OFDM achieves a high spectral efficiency (SE) due to the densely spaced subcarriers with overlapping spectrum and the avoidance of guard bands. Hence, OFDM is adopted in many telecommunication standards such as digital video broadcasting standard for terrestrial broadcasting [3], Long Term Evolution (LTE) and IEEE 802.11x [4].

Recently, the concept of index modulation (IM), which utilizes the index(es) of some transmission entities to carry extra information bits, has been proposed as a competitive alternative digital modulation technique for the future wireless communications [5]. Inspired by the spatial modulation (SM), which considers an M-ary modulated symbol and the index of an active antenna as the information-bearing units [6], a number of researchers also applied the IM principle to OFDM systems. In subcarrier-index modulation (SIM-)OFDM scheme [7], one index bit is offered to each subcarrier and the subcarriers with the majority bit-value are activated to transmit symbols. The number of active subcarriers in each OFDM block is variable and a perfect feedforward link is needed to signify the majority bit-value to the receiver, which make this scheme less practical. Enhanced (E-)SIM-OFDM avoids these drawbacks by employing one index bit to control the states of two consecutive subcarriers [8]. However, the SE of ESIM-OFDM systems is far behind that of OFDM systems if the same constellation size is adopted. A more flexible and efficient IM scheme for OFDM named OFDM with IM (OFDM-IM) is proposed in [9], in which the total subcarriers are divided into several blocks and a subset of subcarriers within each block are activated according to the index bits to transmit M-ary modulated symbols.

The performance of OFDM-IM in terms of bit error rate (BER) [9], minimum Euclidean distance [10], achievable rate [11], and inter-carrier interference [12] is analyzed, revealing the superiority of OFDM-IM over its OFDM counterpart. Due to the advantages of OFDM-IM, plenty of research on OFDM-IM and its variants have emerged. Apart from the maximum-likelihood (ML) detector, some low-complexity detectors, such as log-likelihood ratio detector [9] and greedy detector [13], are proposed to ease the computational burden on the receiver. An upper bound and an approximate expression for the bit error probability (BEP) of OFDM-IM are derived in [14] and [15] assuming ML and energy detection, respectively.

Manuscript received June 9, 2017; revised September 20, 2017 and November 15, 2017; accepted January 9, 2018. Date of publication January 23, 2018; date of current version April 8, 2018. This work was supported in part by the National Natural Science Foundation of China under Grant 61671211, Grant U1701265, and Grant 61501190, in part by the Natural Science Foundation of Guangdong Province under Grant 2016A030311024, in part by the State Major Science and Technology Special Projects under Grant 2016ZX03001009 and Grant 2017ZX03001001, in part by the open research fund of the National Mobile Communications Research Laboratory, Southeast University, under Grant 2017D08, in part by the Turkish Academy of Sciences Outstanding Young Scientist Award Programme (TUBA-GEBIP), and in part by the Scientific Research Projects Foundation, Istanbul Technical University, under Grant 40607. The associate editor coordinating the review of this paper and approving it for publication was M. R. Nakhai. *(Corresponding author: Miaowen Wen.)*

Q. Li and F. Chen are with the School of Electronic and Information Engineering, South China University of Technology, Guangzhou 510640, China (e-mail: eeqiangli@mail.scut.edu.cn; eefjchen@scut.edu.cn).

M. Wen is with the School of Electronic and Information Engineering, South China University of Technology, Guangzhou 510640, China, and also with the National Mobile Communications Research Laboratory, Southeast University, Nanjing 210096, China (e-mail: eemwwen@scut.edu.cn).

E. Basar is with the Faculty of Electrical and Electronics Engineering, Istanbul Technical University, 34469 Istanbul, Turkey (e-mail: basarer@itu.edu.tr).

Color versions of one or more of the figures in this paper are available online at http://ieeexplore.ieee.org.

Digital Object Identifier 10.1109/TWC.2018.2793238

Based on the framework of OFDM-IM, some efforts to increase its SE and diversity order have been made in the literature. On the issue of SE, two generalizations of OFDM-IM, termed OFDM with generalized index modulation 1 (OFDM-GIM1) and OFDM-GIM2, are proposed in [16]. In OFDM-GIM1, the number of active subcarriers in each block is changeable per transmission according to the index bits. In OFDM-GIM2, the IM technique is performed independently on the in-phase (I-) and quadrature (Q-) dimensions, which doubles the amount of index bits of OFDM-IM. Compressed sensing (CS) assisted OFDM-IM [17] improves the SE of OFDM-IM by implementing the conventional IM in a high-dimensional virtual domain, and then compressing the resulting IM symbols into the low-dimensional subcarriers in the frequency domain with the help of the CS technique. In multiple-input multiple-output (MIMO-)OFDM-IM scheme [18], each transmit antenna is equipped with an OFDM-IM transmitter such that the SE increases with the number of transmit antennas. A low-complexity yet near-optimal detector for MIMO-OFDM-IM is designed in [19] based on the sequential Monte Carlo theory. A generic IM scheme for MIMO-OFDM systems, called generalized space and frequency index modulation (GSFIM) is proposed in [20], performing IM in both spatial and frequency domains, and its low-complexity detector is provided in [21] using the multi-stage message passing approach. In dual-mode IM-aided OFDM (DM-OFDM) [22], the "inactive" subcarriers in conventional OFDM-IM are re-activated intentionally to transmit symbols drawn from a constellation different from that employed by the "active" subcarriers.

On the other hand, there already exist some enhanced schemes improving the asymptotic BER performance of OFDM-IM and related systems. In [23], the subcarrier-level interleaving is introduced into OFDM-IM to obtain frequency diversity. In coordinate interleaved (CI-)OFDM-IM [24], the real and imaginary parts of each complex data symbol are transmitted on two different active subcarriers using the CI orthogonal design, which increases the transmit diversity order of ordinary modulation bits from unity to two. To increase the transmit diversity order of index bits solely, the same index bits are fed into two or more blocks in [25]. Space-frequency code is constructed in [26] to improve the transmit diversity of MIMO-OFDM-IM. Finally, the symbol error probability of OFDM-IM with diversity reception is analyzed in [27], in which greedy detection is employed for index bits and ML detection for ordinary modulation bits.

Spread spectrum (SS) signals are widely used for the transmission of digital information over some radio channels to offer message privacy, the capability of combating the determined interference, and code division multiple access (CDMA). The combination of multi-carrier modulation and SS, termed multi-carrier (MC-)SS, is an attempt to take advantage of attributes of both techniques [28]. This combination has prompted a number of new multiple access schemes, such as MC-CDMA and MC direct sequence CDMA (MC-DS-CDMA) [29], [30]. In MC-CDMA, the chips of a spread data symbol are mapped in the frequency scale over several parallel subcarriers. By contrast, MC-DS-CDMA converts the high-rate data stream into parallel low-rate sub-streams, and then the DS spreading is performed on each sub-channel in the time scale with a user-specific spreading code. As a special form of MC-DS-CDMA, single-carrier frequency division multiple access (SC-FDMA) has been adopted in LTE-Advanced for the uplink transmission [31]. In SC-FDMA, the time-domain data symbols are transformed to the frequency domain by a DFT precoder before carrying out the MC modulation. In the above-mentioned MC-CDMA and MC-DS-CDMA, the spreading codes are used to spread symbols and they do not carry any information.

The idea of code IM (CIM), which utilizes the indices of spreading codes to convey additional information bits, is first proposed by the authors of [32]. In their proposed scheme, one additional bit on the I- (Q-) branch is used to select one of two spreading codes, by which the I- (Q-) component of a quadrature phase shift keying (QPSK) symbol is spread. Later, the authors from the same research group generalize CIM in [33] by employing M-PSK/quadrature amplitude modulation (QAM) and allowing the number of available spreading codes to be an arbitrary integral power of two. Furthermore, [34] validates the superiority of CIM over SM in terms of energy efficiency, system complexity, and BER performance, while [35] introduces the CIM technique into differential chaos shift keying scheme to obtain the better BER performance. However, in the existing CIM schemes, DS spreading is performed in the time scale for single-carrier and single-user communications.

Different from the previous CIM schemes, a novel CIM scheme based on OFDM systems, termed index modulated OFDM-SS (IM-OFDM-SS), is proposed in this paper, to improve the diversity order of OFDM-IM and the SE of OFDM-SS. Moreover, a framework of CIM-based multi-user communications is provided. The contributions of this paper are summarized as follows:

- The techniques of IM and SS are combined under the framework of OFDM for the first time. In IM-OFDM-SS, a data symbol is spread across several subcarriers to harvest additional diversity gain by the spreading code that is selected from a predefined set according to the index bits. The idea of IM-OFDM-SS is extended to the multi-code and multi-user scenarios, resulting in the generalized (G-)IM-OFDM-SS and IM-MC-CDMA schemes, respectively.
- We propose a low-complexity maximal ratio combining (MRC) detector for IM-OFDM-SS, which exhibits near-ML error performance. Taking into account the channel estimation errors, an upper bound and an approximate mathematical expression for the BEP of IM-OFDM-SS are derived, assuming ML and MRC detection, respectively.
- Extensive computer simulations are performed, whose results show that IM/GIM-OFDM-SS outperforms the existing OFDM, OFDM-IM, and OFDM-SS schemes significantly. In multi-user communications, IM-MC-CDMA also performs better than the conventional MC-CDMA at the same SEs for either multi-user or single-user detection.

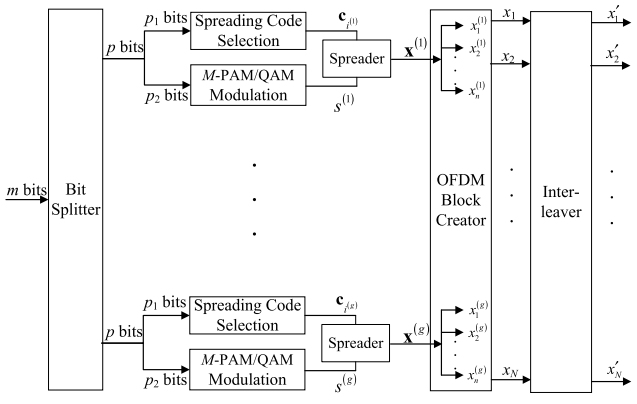

Fig. 1. Transmitter structure of IM-OFDM-SS.

The rest of this paper is organized as follows. Section II gives the system model of IM-OFDM-SS, including the transmitter and receiver structures. The performance in terms of upper bound and mathematical expression for BEP is analyzed in Section III. The idea of IM-OFDM-SS is extended to multi-code and multi-user scenarios in Section IV. Section V presents the computer simulation results and detection complexity comparisons, followed by the conclusion in Section VI.

Notation: Column vectors and matrices are denoted by lowercase and capital bold letters, respectively. Superscripts *, ^{T}, and ^{H} stand for conjugate, transpose, and Hermitian transpose, respectively. $\mathbb{C}$ denotes the ring of complex numbers. $\det(\cdot)$ and $\text{rank}(\cdot)$ return the determinant and rank of a matrix, respectively. $\text{diag}(\cdot)$ transforms a vector into a diagonal matrix. $\mathcal{CN}(0,\sigma^2)$ represents the complex Gaussian distribution with zero mean and variance σ^2. The probability of an event and the probability density function (PDF) are denoted by $\Pr(\cdot)$ and $f(\cdot)$, respectively. $E\{\cdot\}$ denotes the expectation operation. $Q(\cdot)$, $Q_1(\cdot,\cdot)$, and $I_0(\cdot)$ are the Gaussian Q-function, the first-order Marcum Q-function, and the zero-order modified Bessel function of first kind, respectively. $\mathbf{I}_n$ is the $n\times n$ identity matrix. $\lfloor\cdot\rfloor$, $C(\cdot,\cdot)$, and $\|\cdot\|$ denote the floor function, the binomial coefficient, and the Frobenius norm, respectively. We define $[x_1,\ldots,x_n]^T\otimes[y_1,\ldots,y_n]^T=[x_1y_1,\ldots,x_ny_n]^T$.

II. System Model

In this section, we present the transmitter and receiver structures of IM-OFDM-SS.

A. Transmitter

The transmitter structure of IM-OFDM-SS based on the framework of OFDM with N subcarriers is depicted in Fig. 1. To perform IM efficiently, m information bits to be sent for each OFDM frame duration are equally separated into g blocks and IM is performed within $n=N/g$ subcarriers in a block-wise manner. Since the process in all blocks are the same and independent of each other, let us take the β-th block as an example, where $\beta\in\{1,\ldots,g\}$. In the β-th block, the available $p=m/g$ bits are further divided into two parts. The first part consisting of p_1 index bits are used to select the spreading code $\mathbf{c}_{i^{(\beta)}}\in\mathbb{C}^{n\times 1}$ from a predefined set $\mathcal{C}=\{\mathbf{c}_1,\ldots,\mathbf{c}_n\}$, where $i^{(\beta)}\in\{1,\ldots,n\}$ is the index of the spreading code for the β-th block. The second part with $p_2=\log_2(M)$ symbol bits are mapped into a symbol $s^{(\beta)}\in\mathcal{X}$, where $\mathcal{X}$ is an M-ary pulse amplitude modulation (PAM)/QAM constellation having unit average power.

To enable low-complexity detection at the receiver, the spreading codes in $\mathcal{C}$ should be mutually orthogonal, which limits the maximum size of $\mathcal{C}$ to be n. In this paper, Zadoff-Chu and Walsh orthogonal codes are considered. For Walsh codes, we have $\mathcal{C}=\{\mathbf{C}_{:,1},\ldots,\mathbf{C}_{:,n}\}$, where $\mathbf{C}_{:,k}$, $k\in\{1,\ldots,n\}$, represents the k-th column of the $n\times n$ Hadamard matrix. For Zadoff-Chu codes, $\mathcal{C}$ is derived by cyclically shifting a basic Zadoff-Chu sequence by $0,\ldots,n-1$ positions [36]. For n being an even number, we employ the Zadoff-Chu sequence, $\{1,\exp(j\frac{\varpi\pi}{n}),\exp(j\frac{4\varpi\pi}{n}),\ldots,\exp(j\frac{\varpi\pi(n-1)^2}{n})\}$, where ϖ is an integer relatively prime to n. Due to the length constraint of Walsh codes, n is assumed to be an integer power of 2. Therefore, we set $p_1=\log_2(n)$ and the mapping and de-mapping between p_1 bits and $i^{(\beta)}$ can be easily implemented by the natural binary code [37].

Then, the symbol $s^{(\beta)}$ is spread across n subcarriers by the selected spreading code $\mathbf{c}_{i^{(\beta)}}$, yielding

$$\begin{aligned}\mathbf{x}^{(\beta)}&=\left[x_1^{(\beta)},\ldots,x_n^{(\beta)}\right]^T=s^{(\beta)}\mathbf{c}_{i^{(\beta)}}\\&=\left[s^{(\beta)}c_{i^{(\beta)},1},\ldots,s^{(\beta)}c_{i^{(\beta)},n}\right]^T,\end{aligned}\tag{1}$$

where $c_{i^{(\beta)},k}, k\in\{1,\ldots,n\}$ is the k-th element of $\mathbf{c}_{i^{(\beta)}}$. After obtaining $\mathbf{x}^{(\beta)}$ for all β, the OFDM block creator concatenates them, yielding the $N\times 1$ main OFDM block as follows:

$$\begin{aligned}\mathbf{x}_F&=[x_1,\ldots,x_N]^T\\&=\left[x_1^{(1)},\ldots,x_n^{(1)},x_1^{(2)},\ldots,x_n^{(2)},\ldots,x_1^{(g)},\ldots,x_n^{(g)}\right]^T.\end{aligned}\tag{2}$$

To harvest the frequency diversity, an interleaver is adopted, which makes the symbols in the $\mathbf{x}^{(\beta)}$ spaced equally by g subcarriers, obtaining

$$\begin{aligned}\mathbf{x}'_F&=\left[x'_1,\ldots,x'_N\right]^T\\&=\left[x_1^{(1)},\ldots,x_1^{(g)},x_2^{(1)},\ldots,x_2^{(g)},\ldots,x_n^{(1)},\ldots,x_n^{(g)}\right]^T.\end{aligned}\tag{3}$$

Afterwards, the remaining procedures are the same as those of classical OFDM, which are omitted in Fig. 1. First, $\mathbf{x}'_F$ is processed by the inverse fast Fourier transform (IFFT), yielding the time-domain OFDM block

$$\mathbf{x}_T=[X_1,\ldots,X_N]^T=\frac{1}{\sqrt{N}}\mathbf{W}_N^H\mathbf{x}'_F,\tag{4}$$

where $\mathbf{W}_N$ is the $N\times N$ DFT matrix with $\mathbf{W}_N^H\mathbf{W}_N=N\mathbf{I}_N$. A length-$L$ cyclic prefix (CP) $[X_{N-L+1},\ldots,X_N]^T$ is added to the beginning of $\mathbf{x}_T$. After the parallel-to-serial and digital-to-analog conversions, the data is transmitted over the frequency-selective Rayleigh fading channel, whose impulse response is given by $\mathbf{h}_T=\left[h_{T,1},\ldots,h_{T,\upsilon}\right]^T$, where υ is the number of channel taps and each entry of $\mathbf{h}_T$ is a circularly symmetric

complex Gaussian random variable following the distribution $\mathcal{CN}(0, 1/\upsilon)$. Note that L is chosen to be larger than υ to combat the intersymbol interference.

At the receiver, N-point FFT and de-interleaving are carried out in sequence after discarding the CP of the received signal. Hence, the input-output relationship in the frequency domain for the β-th block is given by

$$\mathbf{y}^{(\beta)} = \mathbf{X}^{(\beta)}\mathbf{h}^{(\beta)} + \mathbf{w}^{(\beta)}, \tag{5}$$

where $\mathbf{X}^{(\beta)} = \mathrm{diag}(\mathbf{x}^{(\beta)})$, $\mathbf{h}^{(\beta)}$ is the $n \times 1$ frequency-domain channel vector, and $\mathbf{w}^{(\beta)} \in \mathbb{C}^{n\times 1}$ is the noise vector in the frequency domain with the distribution $\mathcal{CN}(\mathbf{0}, N_0\mathbf{I}_n)$. Note that the frequency-domain channel vector is given by $\mathbf{h}_F = \mathbf{W}_N\mathbf{h}_T^0$, where $\mathbf{h}_T^0$ is the length-N zero-padded version of the vector $\mathbf{h}_T$, namely $\mathbf{h}_T^0 = [\mathbf{h}_T{}^T, 0, \ldots, 0]^T$. Hence, with de-interleaving, $\mathbf{h}^{(\beta)} = [h_{F,\beta}, h_{F,\beta+g}, \ldots, h_{F,\beta+(n-1)g}]^T$, and the elements of $\mathbf{h}^{(\beta)}$ can be viewed as independent and identically distributed (i.i.d.), which means $\mathbf{h}^{(\beta)} \sim \mathcal{CN}(\mathbf{0}, \mathbf{I}_n)$. We rewrite (5) in a scalar form as

$$y_k^{(\beta)} = s^{(\beta)}h_k^{(\beta)}c_{i^{(\beta)},k} + w_k^{(\beta)}, \quad k = 1, \ldots, n, \tag{6}$$

where $y_k^{(\beta)}$, $h_k^{(\beta)}$, and $w_k^{(\beta)}$ are the samples of $\mathbf{y}^{(\beta)}$, $\mathbf{h}^{(\beta)}$, and $\mathbf{w}^{(\beta)}$, respectively, at the k-th subcarrier. We define the average signal-to-noise ratio (SNR) per subcarrier as $\gamma = 1/N_0$. The SE of IM-OFDM-SS scheme regardless of the CP overhead is given by (bps/Hz)

$$\mathcal{E}_{\mathrm{IM-OFDM-SS}} = (p_1 + p_2)/n = \log_2(Mn)/n, \tag{7}$$

while the SE of OFDM-SS is $\mathcal{E}_{\mathrm{OFDM-SS}} = \log_2(M)/n$, from which we observe that IM-OFDM-SS achieves a higher SE than OFDM-SS.

B. Receiver

In this subsection, we address the detection problem of IM-OFDM-SS by taking into account the effects of channel estimation errors. Two different types of detectors are provided for the IM-OFDM-SS scheme, including the ML detector and the MRC detector, whose theoretical error performance will be analyzed in Section III. Since the encoding processes for all blocks are identical and independent, the detection can be performed block by block. To simplify notations, in the sequel we focus only on one block and omit the superscript (β).

In practical systems, the channel vector $\mathbf{h}$ is estimated at the receiver as [38]

$$\bar{\mathbf{h}} = \mathbf{h} + \mathbf{h}_e, \tag{8}$$

where $\mathbf{h}_e \in \mathbb{C}^{n\times 1}$ represents the vector of channel estimation errors with the distribution $\mathcal{CN}(\mathbf{0}, \sigma_e^2\mathbf{I}_n)$, and it is independent of $\mathbf{h}$. Hence, $\bar{\mathbf{h}}$, whose elements are $\bar{h}_k, k = 1, \ldots, n$, follows the distribution $\mathcal{CN}(\mathbf{0}, (1+\sigma_e^2)\mathbf{I}_n)$. According to the first-order autoregressive model and (8), $\mathbf{h}$ can be given by [39]

$$\mathbf{h} = \rho\bar{\mathbf{h}} + \mathbf{u}, \tag{9}$$

where $\rho = 1/(1+\sigma_e^2)$ is the correlation coefficient between the elements of $\mathbf{h}$ and $\bar{\mathbf{h}}$, and $\mathbf{u} = [u_1, \ldots, u_n]^T = (1-\rho)\mathbf{h} - \rho\mathbf{h}_e$, which is independent of $\bar{\mathbf{h}}$ with the distribution $\mathcal{CN}(\mathbf{0}, (1-\rho)\mathbf{I}_n)$.

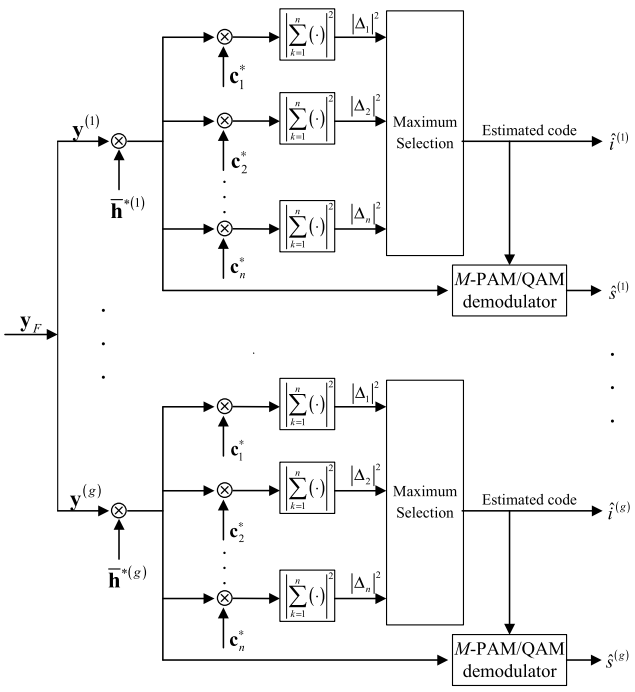

Fig. 2. MRC detector for IM-OFDM-SS.

1) ML Detector: From (5), the mismatched ML detector makes a joint decision on the index of spreading code and the constellation symbol by searching all possible combinations of them, namely

$$(\hat{i}, \hat{s}) = \arg\min_{i,s} \left\|\mathbf{y} - \mathbf{X}\bar{\mathbf{h}}\right\|^2. \tag{10}$$

Then, the corresponding p information bits can be readily recovered from $\hat{i}$ and $\hat{s}$. Obviously, the ML detector should search all Mn possible $\mathbf{X}$ to find out the one that minimizes the ML metric, which results in the computational complexity in terms of complex multiplications of order $\sim \mathcal{O}(Mn)$ per block. Although the complexity of ML detector is acceptable for moderate values of n and M, it still poses intolerable computational burden in the case of multi-user communications, as we will see in Section IV. Therefore, the design of a detector with complexity lower than that of ML detector is demanding.

2) MRC Detector: In this detector, the detection process is divided into two steps, as described in Fig. 2. The first step is to estimate the selected spreading code, and the second step is to detect the information symbol based on the spreading code estimated in the first step.

At the first stage, $\mathbf{y}$ is fed into n one-tap equalizers in parallel, each of which is simply realized by one complex-valued multiplication per subcarrier. According to MRC, the l-th equalizer for the k-th subcarrier is given by $z_{l,k} = \bar{h}_k^* c_{l,k}^*$, and combining n subcarriers, yields

$$\Delta_l = \sum_{k=1}^{n} z_{l,k}y_k, \quad l = 1, \ldots, n. \tag{11}$$

Then, the squared values of the outputs of n branches are compared to determine the index of the selected spreading code via

$$\hat{i} = \arg\max_l |\Delta_l|^2. \tag{12}$$

After obtaining $\hat{i}$, at the second stage, the information symbol s can be estimated readily via

$$\hat{s} = \arg\min_{s} \left| \sum_{k=1}^{n} z_{\hat{i},k} y_k - s \sum_{k=1}^{n} \left|\bar{h}_k\right|^2 \right|^2. \tag{13}$$

From the description above, complex multiplications of order $\sim \mathcal{O}(n)$ and $\mathcal{O}(M)$ are involved at the first and second stages, respectively. Considering the two-stage detection process is performed successively, we conclude that the overall computational complexity of the MRC detector is of order $\sim \mathcal{O}(n+M)$, which is very beneficial in multi-user communications. In addition, since MRC is able to obtain a large minimum distance among $|\Delta_l|^2, l = l, \ldots, n$, the spreading code index detection of the MRC detector has a comparable reliability to that of the ML detector. Once the spreading code index is detected correctly, the second step of the MRC detector becomes the ML detection. Therefore, the MRC detector has the ability to achieve the near-ML performance, which will be validated in Section V.

Remark 1: Channel estimation errors can be regarded as interference, which lowers the signal-to-interference-plus-noise ratio (SINR). Moreover, with increasing SNR, the SINR converges towards a constant. Therefore, for the ML detection, channel estimation errors deteriorate seriously the performance of the joint detection of the spreading code index and the M-ary symbol. Particularly, an error floor is observed in the high SNR region. For the MRC detection, channel estimation errors narrow the minimum distance among $|\Delta_l|^2$ at the first stage, which results in a higher error probability of detecting the spreading code index. The second stage detection also becomes worse as a result of a lower SINR. Similar to the ML detector, the MRC detector creates an error floor at high SNR. In the presence of channel estimation errors, since the spreading code index is estimated first by comparing n possible energy-like metrics, i.e., $|\Delta_l|^2$, the MRC detector is less susceptible to the channel estimation errors, than the ML detector. Additionally, the MRC detector exhibits near-ML performance at much lower complexity. We conclude that the MRC detector is more suitable for systems with channel estimation errors.

III. Performance Analyses

In this section, we derive an upper bound and an analytical expression for the BEP of IM-OFDM-SS in the presence of channel estimation errors, assuming ML and MRC detection, respectively.

A. BEP Upper Bound for the ML Detector

In the presence of channel estimation errors, the conditional pairwise error probability (PEP) can be calculated as [9]

$$\Pr\left(\mathbf{X} \to \hat{\mathbf{X}} \,|\bar{\mathbf{h}}\right) = Q\left(\frac{\left\| \left(\mathbf{X} - \hat{\mathbf{X}}\right) \bar{\mathbf{h}} \right\|^2}{\sqrt{2\sigma_e^2 \left\| \mathbf{X}^H \left(\mathbf{X} - \hat{\mathbf{X}}\right) \bar{\mathbf{h}} \right\|^2 + 2N_0 \left\| \left(\mathbf{X} - \hat{\mathbf{X}}\right) \bar{\mathbf{h}} \right\|^2}} \right), \tag{14}$$

where $\hat{\mathbf{X}}$ is the estimate of $\mathbf{X}$. Since $|c_{i,k}|^2 = 1$ for any i, $k \in \{1, \ldots, n\}$, we have

$$\begin{aligned} \left\| \mathbf{X}^H (\mathbf{X} - \hat{\mathbf{X}}) \bar{\mathbf{h}} \right\|^2 &= \sum_{k=1}^{n} \left| s c_{i,k} \right|^2 \left| \left(x_k - \hat{x}_k\right) \bar{h}_k \right|^2 \\ &= \frac{1}{n} \|\mathbf{x}\|^2 \left\| (\mathbf{X} - \hat{\mathbf{X}}) \bar{\mathbf{h}} \right\|^2. \end{aligned} \tag{15}$$

Hence, (14) can be expressed as

$$\Pr\left(\mathbf{X} \to \hat{\mathbf{X}} \,|\bar{\mathbf{h}}\right) = Q\left(\sqrt{\frac{\left\| \left(\mathbf{X} - \hat{\mathbf{X}}\right) \bar{\mathbf{h}} \right\|^2}{2N_0 + 2\sigma_e^2 \|\mathbf{x}\|^2 / n}} \right). \tag{16}$$

By following the method presented in [9], we obtain an approximate unconditional PEP

$$\Pr\left(\mathbf{X} \to \hat{\mathbf{X}}\right) \approx \frac{1/12}{\det\left(\mathbf{I}_n + q_1 \bar{\mathbf{K}}_n \mathbf{A}\right)} + \frac{1/4}{\det\left(\mathbf{I}_n + q_2 \bar{\mathbf{K}}_n \mathbf{A}\right)}, \tag{17}$$

where $q_1 = n/(4nN_0 + 4\|\mathbf{x}\|^2 \sigma_e^2)$, $q_2 = n/(3nN_0 + 3\|\mathbf{x}\|^2 \sigma_e^2)$, and $\mathbf{A} = (\mathbf{X} - \hat{\mathbf{X}})^H (\mathbf{X} - \hat{\mathbf{X}})$. Then, according to the union bounding technique, a BEP upper bound can be given by

$$P_u \le \frac{1}{p 2^p} \sum_{\mathbf{X}} \sum_{\hat{\mathbf{X}}} \Pr\left(\mathbf{X} \to \hat{\mathbf{X}}\right) N\left(\mathbf{X}, \hat{\mathbf{X}}\right), \tag{18}$$

where $N(\mathbf{X}, \hat{\mathbf{X}})$ is the number of erroneous bits when $\mathbf{X}$ is detected as $\hat{\mathbf{X}}$.

At high SNR, (18) approximates to

$$P_u \approx \frac{1}{p 2^p} \sum_{\mathbf{X}, \hat{\mathbf{X}}} \left(\prod_{\omega=1}^{d} \lambda_\omega \left(\bar{\mathbf{K}}_n \mathbf{A}\right) \right)^{-1} \times \left(\frac{1}{12 q_1^d} + \frac{1}{4 q_2^d} \right) N\left(\mathbf{X}, \hat{\mathbf{X}}\right), \tag{19}$$

where $d = \text{rank}(\bar{\mathbf{K}}_n \mathbf{A}) = \text{rank}(\mathbf{A})$ and $\lambda_\omega(\bar{\mathbf{K}}_n \mathbf{A})$, $\omega = 1, \ldots, d$, are the nonzero eigenvalues of $\bar{\mathbf{K}}_n \mathbf{A}$.

Remark 2: The diversity order achieved by IM-OFDM-SS without channel estimation errors is given by $d_{\min} = \min \text{rank}(\mathbf{A})$. Recalling that $\mathbf{A} = (\mathbf{X} - \hat{\mathbf{X}})^H (\mathbf{X} - \hat{\mathbf{X}}) = \text{diag}(|s\mathbf{c}_i - \hat{s}\mathbf{c}_{\hat{i}}|^2)$, when the receiver correctly detects the spreading code index and makes a decision error for the M-ary symbol, we have $\mathbf{A} = \text{diag}(|s\mathbf{c}_i - \hat{s}\mathbf{c}_i|^2)$ that has no zero diagonal element, by which we are led to $d_{\min} = n$. When the transmitted spreading code is detected erroneously, for Zadoff-Chu codes with $n > 2$ or Walsh codes, $d_{\min}$ is achieved in the case of the correct estimation of the M-ary symbol. For this type of error event, we have $\mathbf{A} = |s|^2 \text{diag}(|\mathbf{c}_i - \mathbf{c}_i|^2)$. Hence, $d_{\min}$ is the minimum Hamming distance between any two different orthogonal codes drawn from $\mathcal{C}$, which can be shown to be $n/2$. On the other hand, for Zadoff-Chu codes with $n = 2$, the Hamming distance between two codes is 2. Hence, for M-PAM, we have $d_{\min} = 2$, while for M-QAM, since there exist combinations of s and $\hat{s}$ that generate $d = 1$, we have $d_{\min} = 1$. To sum up, the achievable diversity order

of IM-OFDM-SS is given by

$$d_{\min} = \begin{cases} 2, & \text{for } n = 2, M\text{-PAM, and Zadoff-Chu codes,} \\ n/2, & \text{otherwise.} \end{cases} \tag{20}$$

Compared with classical OFDM and OFDM-IM, a higher diversity order is obtained by IM-OFDM-SS when $n \geq 4$. Besides, IM-OFDM-SS provides a flexible trade-off between the SE and the diversity order by adjusting n.

B. BEP Analysis for the MRC Detector

Motivated by the two-stage nature of the MRC detector, we observe that the bit errors of IM-OFDM-SS result from two error cases:

(i) an incorrect index estimation of the spreading code;
(ii) a correct index estimation of the spreading code.

In case (i), due to the incorrect detection of the transmitted spreading code, bit errors occur in both p_1 index and p_2 ordinary modulation bits. In case (ii), although the index of the transmitted spreading code is correctly detected, there is still a probability of error in p_2 ordinary modulation bits. Since cases (i) and (ii) are complementary, the overall BEP can be evaluated as

$$P_b = P_{cd} P_{b,\mathrm{i}} + (1 - P_{cd}) P_{b,\mathrm{ii}}, \tag{21}$$

where $P_{b,\mathrm{i}}$ and $P_{b,\mathrm{ii}}$ are the BEPs for cases (i) and (ii), respectively, and P_{cd} is the erroneous spreading code detection probability.

In case (i), the index of the spreading code may be detected incorrectly as one of the remaining $n-1$ indices with equal probability $P_{cd}/(n-1)$. A different incorrect index may result in a different number of erroneous bits, and it can be readily figured out that there are in total $C(p_1, t)$ error events that correspond to t erroneous index bits, where $t \in \{1, \ldots, p_1\}$. On the other hand, consider that at high SNR, demodulating an M-PAM/QAM Gray encoded symbol based on an incorrectly detected spreading code mostly yields one erroneous bit [8]. Therefore, we have

$$P_{b,\mathrm{i}} \approx \frac{1}{p}\left(\frac{1}{n-1}\sum_{t=1}^{p_1} t C(p_1, t) + 1\right). \tag{22}$$

In case (ii), $P_{b,\mathrm{ii}}$ can be easily formulated as

$$P_{b,\mathrm{ii}} = \frac{p_2}{p} P_{sb}, \tag{23}$$

where P_{sb} is the BEP of M-ary PAM/QAM demodulation over n i.i.d. Rayleigh fading channels.

From (21)-(23), the overall BEP for the MRC detector of IM-OFDM-SS can be derived once the P_{cd} and P_{sb} are obtained. Next, we will deal with the calculation of P_{cd} and P_{sb}.

1) Erroneous Spreading Code Detection Probability (P_{cd}): At the first stage, the receiver selects the index with the maximum value of $|\Delta_l|^2$ as the index of the transmitted spreading code. Since each spreading code is selected equiprobably at the transmitter, without loss of generality, we assume $\mathbf{c}_i$ is transmitted. Then, the error probability conditioned on the symbol s and channel vector $\bar{\mathbf{h}}$ is given by

$$\begin{aligned} P_{cd|s,\bar{\mathbf{h}}} &= 1 - P\left(|\Delta_i|^2 > |\Delta_1|^2, \ldots, |\Delta_i|^2 > |\Delta_n|^2\right) \\ &\approx 1 - \prod_{\substack{l=1 \\ l\neq i}}^{n} P(D_{il} > 0) \\ &= 1 - \prod_{\substack{l=1 \\ l\neq i}}^{n} [1 - P(D_{il} \leq 0)], \end{aligned} \tag{24}$$

where $D_{il} = |\Delta_i|^2 - |\Delta_l|^2$. With (9), the received signal y_k in (6) can be rewritten as

$$y_k = \rho s \bar{h}_k c_{i,k} + s c_{i,k} u_k + w_k, \quad k = 1, \ldots, n, \tag{25}$$

which leads to

$$\Delta_i = \rho s \sum_{k=1}^{n} |\bar{h}_k|^2 + s \sum_{k=1}^{n} \bar{h}_k^* u_k + \sum_{k=1}^{n} \bar{h}_k^* c_{i,k}^* w_k \tag{26}$$

and

$$\Delta_l = \rho s \sum_{k=1}^{n} |\bar{h}_k|^2 c_{l,k}^* c_{i,k} + s \sum_{k=1}^{n} \bar{h}_k^* c_{l,k}^* c_{i,k} u_k + \sum_{k=1}^{n} \bar{h}_k^* c_{l,k}^* w_k, \tag{27}$$

for $i \neq l$. It is easy to observe that Δ_i and Δ_l are two complex Gaussian random variables with mean values

$$\mu_i = \rho s \sum_{k=1}^{n} |\bar{h}_k|^2 \quad \text{and} \quad \mu_l = \rho s \sum_{k=1}^{n} |\bar{h}_k|^2 c_{l,k}^* c_{i,k}, \tag{28}$$

respectively. The variances of the real and imaginary components of Δ_i and Δ_l are the same, given by

$$\sigma_{ii}^2 = \sigma_{ll}^2 = \frac{1}{2}\left(|s|^2(1-\rho) + N_0\right) \sum_{k=1}^{n} |\bar{h}_k|^2. \tag{29}$$

The cross-covariance between Δ_i and Δ_l is defined as

$$\begin{aligned} \sigma_{il}^2 &= \frac{1}{2} E\left\{(\Delta_i - \mu_i)(\Delta_l - \mu_l)^*\right\} \\ &= \frac{1}{2}\left(|s|^2(1-\rho) + N_0\right) \sum_{k=1}^{n} |\bar{h}_k|^2 c_{l,k} c_{i,k}^*. \end{aligned} \tag{30}$$

Recall that the decision metric D_{il} in (24) is a special quadratic form of complex Gaussian random variables. According to [40, Eq. (9A.10)], we have

$$P(D_{il} \leq 0) = Q_1(a, b) - \frac{1}{2}\exp\left(-\frac{a^2+b^2}{2}\right) I_0(ab), \tag{31}$$

where

$$a = \left[\frac{\nu(\xi_1 \nu - \xi_2)}{2}\right]^{1/2}, \quad b = \left[\frac{\nu(\xi_1 \nu + \xi_2)}{2}\right]^{1/2}, \tag{32}$$

with

$$\begin{aligned} \nu &= \sqrt{\frac{1}{4\left(\sigma_{ii}^2 \sigma_{ll}^2 - |\sigma_{il}^2|^2\right)}}, \\ \xi_1 &= 2\left(|\mu_i|^2 \sigma_{ll}^2 + |\mu_l|^2 \sigma_{ii}^2 - \mu_i^* \mu_l \sigma_{il}^2 - \mu_i \mu_l^* \left(\sigma_{il}^2\right)^*\right), \\ \xi_2 &= |\mu_i|^2 - |\mu_l|^2. \end{aligned} \tag{33}$$

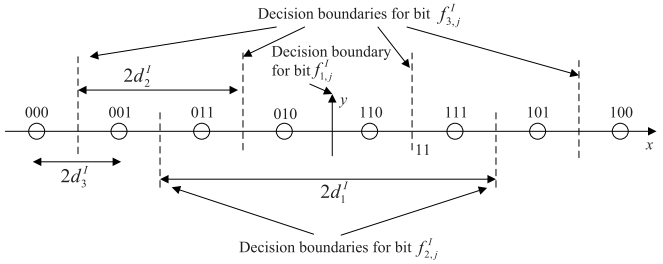

Fig. 3. 8-PAM constellation.

After obtaining $P(D_{il} \leq 0)$ for all $l = 1, \ldots, n$ and $l \neq i$, $P_{cd|s,\bar{\mathbf{h}}}$ can be calculated by (24). Averaging $P_{cd|s,\bar{\mathbf{h}}}$ over s and $\bar{\mathbf{h}}$, the unconditional erroneous spreading code detection probability can be expressed as

$$P_{cd} = E_{s,\bar{\mathbf{h}}}\left\{P_{cd|s,\bar{\mathbf{h}}}\right\} = \frac{1}{M}\sum_{s}\int_{\bar{\mathbf{h}}} P_{cd|s,\bar{\mathbf{h}}}\, f\left(\bar{\mathbf{h}}\right) d\bar{\mathbf{h}}. \quad (34)$$

Unfortunately, due to the complexity of $P_{cd|s,\bar{\mathbf{h}}}$, a closed-form expression for P_{cd} is not available. However, the calculation of P_{cd} can be easily performed in computationally efficient softwares such as MATLAB using numerical evaluation.

2) BEP of M-ary PAM/QAM Demodulation (P_{sb}): Here, we derive closed-form BEP expressions for M-PAM and M-QAM over n i.i.d. Rayleigh fading channels when the n-branch MRC receiver is used. With error-free detection of the spreading code, (25) can rewritten as

$$y_k = \rho s \bar{h}_k + \underbrace{s u_k + w_k}_{\text{Equivalent noise}}, \quad k = 1, \ldots, n, \quad (35)$$

which shows that the equivalent noise depends on the transmitted symbol.

Let us first consider the M-PAM constellation and assume that M-PAM symbols are transmitted over the I- channel. Fig. 3 illustrates the 8-PAM constellation with the distance vector $\mathbf{d}^I = [d^I_1, d^I_2, \ldots, d^I_{p^I_2}]^T = [2^{p^I_2-1}, 2^{p^I_2-2}, \ldots, 1]^T d^I_{p^I_2}$, where $p^I_2 = 3$ and $d^I_{p^I_2}$=1. Let us label the constellation points from the left to right with integers counting from 0 to $M-1$, such that the Gray code $(f^I_{1,j}, f^I_{2,j}, \ldots, f^I_{p^I_2,j})$ for the j-th $(j = 0, \ldots, M-1)$ point in the constellation is given by

$$\begin{aligned} f^I_{1,j} &= b^I_{1,j}, \\ f^I_{t,j} &= b^I_{t,j} + b^I_{t-1,j} \mod 2, \ t = 2, \ldots, p^I_2, \end{aligned} \quad (36)$$

where $(b^I_{1,j}, b^I_{b,j}, \ldots, b^I_{p^I_2,j})$ is the binary representation of j. Some other parameters, such as the average symbol energy, the positions of the symbols in the constellation, and the decision boundaries for each bit, can also be obtained from the constellation [41]:

- The average symbol energy is given by $E_s = \left(\mathbf{d}^I\right)^T \mathbf{d}^I$.
- The positions of M symbols in the constellation form the vector $\mathbf{d}^{I'}_s = [d^{I'}_{s,0}, \ldots, d^{I'}_{s,M-1}]^T$, where

$$d^{I'}_{s,j} = \sum_{t=1}^{p^I_2}\left(2b^I_{t,j} - 1\right) d^I_t, \quad j = 0, \ldots, M-1, \quad (37)$$

  and the constellation with unit average power can be obtained by $\mathbf{d}^I_s = [d^I_{s,0}, \ldots, d^I_{s,M-1}]^T = \mathbf{d}^{I'}_s/\sqrt{E_s}$.
- The l-th decision boundary of the t-th bit is defined as

$$B^I_{t,l} = \frac{d^I_{s,(2l-1)2^{p^I_2-t}} + d^I_{s,(2l-1)2^{p^I_2-t}+1}}{2}, \quad l = 1, \ldots, 2^{t-1}. \quad (38)$$

For the first bit of j-th symbol, i.e., $f^I_{1,j}$, considering (35) and the decision boundary for $f^I_{1,j}$ at the y-axis, an error will take place if the equivalent noise exceeds the absolute value of $\rho d^I_{s,j}$ when $f^I_{1,j}$ is 0. Therefore, the error probability, $P_{sb}(f^I_{1,j})$, for bit $f^I_{1,j}$ is of the form

$$P_{sb}\left(f^I_{1,j}\right) = F\left(-\rho d^I_{s,j}\right), \quad (39)$$

where $F(x)$ is given by (40), shown at the bottom of this page, with

$$\mu_c(x) = \sqrt{\frac{\bar{\gamma}x^2}{1+\bar{\gamma}x^2}}, \quad \bar{\gamma} = 1/\left[\rho\left((1-\rho)(d^I_{s,j})^2 + N_0\right)\right]. \quad (41)$$

The proof of (39) is provided in Appendix. When $f^I_{1,j}$ is 1, the error probability $P_{sb}(f^I_{1,j})$ becomes

$$P_{sb}\left(f^I_{1,j}\right) = F\left(\rho d^I_{s,j}\right) = 1 - F\left(-\rho d^I_{s,j}\right). \quad (42)$$

Putting (39) and (42) together, we obtain a generic expression for $P_{sb}(f^I_{1,j})$, namely

$$P_{sb}\left(f^I_{1,j}\right) = f^I_{1,j} + (-1)^{f^I_{1,j}} F\left(B^I_{1,1} - \rho d^I_{s,j}\right). \quad (43)$$

The analysis given above for $f^I_{1,j}$ can be easily generalized to that for $f^I_{t,j}\left(t = 2, \ldots, p^I_2\right)$ by taking into account the effects of multiple decision boundaries where the sign of $F(\cdot)$ should be changed one time whenever a new boundary is detected, resulting in

$$P_{sb}\left(f^I_{t,j}\right) = f^I_{t,j} + (-1)^{f^I_{t,j}} \sum_{l=1}^{2^{t-1}} (-1)^{l+1} F\left(B^I_{t,l} - \rho d^I_{s,j}\right). \quad (44)$$

$$F(x) = \begin{cases} \left(\dfrac{1-\mu_c(x)}{2}\right)^n \displaystyle\sum_{k=0}^{n-1} C(n-1+k,k)\left(\dfrac{1+\mu_c(x)}{2}\right)^k, & x \geq 0 \\ 1 - \left(\dfrac{1-\mu_c(x)}{2}\right)^n \displaystyle\sum_{k=0}^{n-1} C(n-1+k,k)\left(\dfrac{1+\mu_c(x)}{2}\right)^k, & x < 0 \end{cases} \quad (40)$$

By averaging (44) over those symbols in the left of the plane, we obtain the average error probability for the t-th bit ($t = 1, \ldots, p_2^I$) as

$$P_{sb}\left(f_t^I\right) = \frac{2}{M}\sum_{j=0}^{M/2-1}\Bigg[f_{t,j}^I + (-1)^{f_{t,j}^I} \times \sum_{l=1}^{2^{t-1}}(-1)^{l+1}F\left(B_{t,l}^I - \rho d_{s,j}^I\right)\Bigg]. \quad (45)$$

Finally, because of the equal transmit probability for each bit, a closed-form BEP expression for M-PAM over n i.i.d. Rayleigh fading channels can be derived as

$$P_{sb} = \frac{2}{M\log_2(M)}\sum_{t=1}^{\log_2(M)}\sum_{j=0}^{M/2-1}\Bigg[f_{t,j}^I + (-1)^{f_{t,j}^I} \times \sum_{l=1}^{2^{t-1}}(-1)^{l+1} F\left(B_{t,l}^I - \rho d_{s,j}^I\right)\Bigg]. \quad (46)$$

Next, we consider the case for M-QAM constellation with $M = 2^{p_2^I + p_2^Q}$, where p_2^I and p_2^Q bits are transmitted over the I- and Q- channels, respectively. Since the M-QAM constellation can be regarded as two PAM constellations in quadrature with one being $2^{p_2^I}$-PAM in the I- channel and the other being $2^{p_2^Q}$-PAM in the Q- channel, the BEP analyses for M-QAM are similar to those for the M-PAM addressed above.

Before the presentation of the BEP expression for M-QAM, we redefine some parameters for the Q- channel including the Gray code, distance vector, position vector, and decision boundaries, in a similar fashion. Note that for M-QAM the average symbol energy becomes

$$E_s = \left(\mathbf{d}^I\right)^T \mathbf{d}^I + \left(\mathbf{d}^Q\right)^T \mathbf{d}^Q, \quad (47)$$

and the $\bar{\gamma}$ in (41) should be revised as $\bar{\gamma} = 1/\rho[(1-\rho)((d_{s,j}^I)^2 + 1/2) + N_0]$, where for the instantaneous power of the symbol over Q- channel, we used the average power value, i.e., $1/2$ for simplicity.

Therefore, the BEP for M-QAM over n i.i.d. Rayleigh fading channels is derived as (48) [42], shown at the bottom of this page.

After obtaining P_{cd} and P_{sb}, the overall BEP for the MRC detector of IM-OFDM-SS can be derived by substituting (22) and (23) into (21).

IV. Extension to Multi-Code and Multi-User Scenarios

In this section, we extend the idea of IM-OFDM-SS to multi-code and multi-user scenarios.

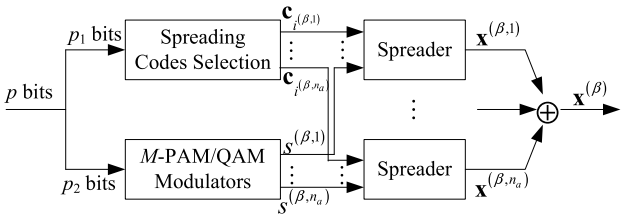

Fig. 4. The IM operation of the GIM-OFDM-SS transmitter for the β-th block.

A. Extension to Multi-Code Scenario

Aiming at increasing the SE of IM-OFDM-SS, in this subsection, we propose the GIM-OFDM-SS scheme, in which multiple spreading codes are activated for one user. The transmitter structure of GIM-OFDM-SS is the same as that of IM-OFDM-SS except that the IM process is replaced by the multi-code version. We highlight the IM operation for the β-th block in Fig. 4.

In GIM-OFDM-SS, for the β-th block, n_a spreading codes, $\{\mathbf{c}_{i^{(\beta,1)}}, \ldots, \mathbf{c}_{i^{(\beta,n_a)}}\}$, are activated according to the $p_1 = \lfloor \log_2(C(n, n_a)) \rfloor$ index bits via the combinatorial method [9], while $p_2 = n_a \log_2(M)$ symbol bits determine n_a M-ary PAM/QAM symbols, $\{s^{(\beta,1)}, \ldots, s^{(\beta,n_a)}\}$. Then, $s^{(\beta,\tau)}$ is spread by $\mathbf{c}_{i^{(\beta,\tau)}}, \tau = 1, \ldots, n_a$. The summation of the spread symbols is given by $\mathbf{x}^{(\beta)} = \sum_{\tau=1}^{n_a} s^{(\beta,\tau)} \mathbf{c}_{i^{(\beta,\tau)}}$. Afterwards, the remaining procedures are the same as that of IM-OFDM-SS. Obviously, the SE of GIM-OFDM-SS increases to (bps/Hz)

$$\mathcal{E}_{\text{GIM-OFDM-SS}} = \frac{\lfloor \log_2(C(n, n_a)) \rfloor + n_a \log_2(M)}{n}. \quad (49)$$

At the receiver, both the indices of n_a spreading codes and n_a symbols should be estimated for each block. Likewise, the ML and MRC detectors can be derived accordingly by modifying (10)-(13).

B. Extension to Multi-User Scenario

In this subsection, the idea of IM-OFDM-SS is extended to multi-user communications, giving rise to the scheme of IM-MC-CDMA. Fig. 5 shows the block diagram of IM-MC-CDMA, where T users and the base station are all equipped with the transceivers of IM-OFDM-SS. To distinguish each user and enable IM at the same time, the spreading code set $\mathcal{C}$ is partitioned into T subsets each of which contains n/T elements, and each user selects the spreading code from the corresponding subset according to its index bits. Therefore,

$$P_{sb} = \frac{1}{\log_2(M)}\Bigg\{2^{1-p_2^I}\sum_{t=1}^{p_2^I}\sum_{j=0}^{2^{p_2^I-1}-1}\left[f_{t,j}^I + (-1)^{f_{t,j}^I}\sum_{l=1}^{2^{t-1}}(-1)^{l+1}F\left(B_{t,l}^I - \rho d_{s,j}^I\right)\right] + 2^{1-p_2^Q}\sum_{t=1}^{p_2^Q}\sum_{j=0}^{2^{p_2^Q-1}-1}\left[f_{t,j}^Q + (-1)^{f_{t,j}^Q}\sum_{l=1}^{2^{t-1}}(-1)^{l+1}F\left(B_{t,l}^Q - \rho d_{s,j}^Q\right)\right]\Bigg\}. \quad (48)$$

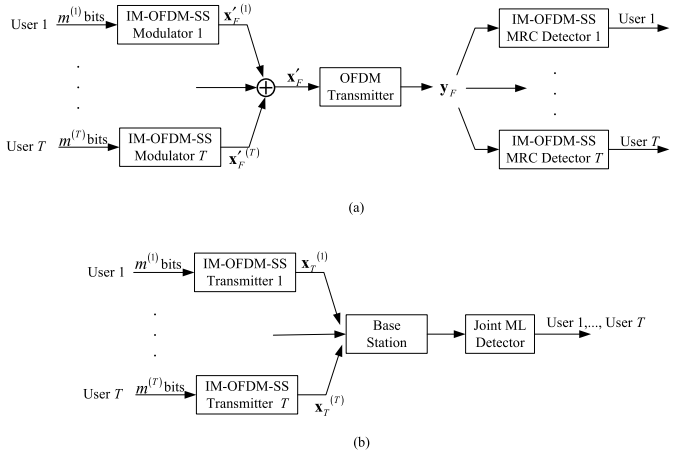

Fig. 5. Block diagram of IM-MC-CDMA for (a) downlink and (b) uplink.

the overall SE of IM-MC-CDMA is given by (bps/Hz)

$$\mathcal{E}_{\text{IM-MC-CDMA}} = \frac{T}{n}\log_2\left(Mn/T\right). \tag{50}$$

In the downlink, without loss of generality, we focus on the detection problem at the first user, whose received signal is

$$y_k = h_k \sum_{t=1}^{T} s^{(t)} c_{i^{(t)},k} + w_k^{(1)}, \quad k = 1, \ldots, n, \tag{51}$$

where $s^{(t)}$, $c_{i^{(t)},k}$, and $w_k^{(t)}$ are the transmitted symbol, selected spreading code, and noise, respectively, on the k-th subcarrier. From (51), both the optimal ML detection and single-user detection can be employed to detect the data.

The ML detector estimates the data of all T users jointly via

$$\left\{\hat{s}^{(1)}, \hat{i}^{(1)}, \ldots, \hat{s}^{(T)}, \hat{i}^{(T)}\right\} = \underset{\{s^{(1)},i^{(1)},\ldots,s^{(T)},i^{(T)}\}}{\arg\min} \sum_{k=1}^{n} \left| y_k - \bar{h}_k \sum_{t=1}^{T} s^{(t)} c_{i^{(t)},k} \right|^2. \tag{52}$$

The computational complexity of (52) is of order $\sim\mathcal{O}((Mn/T)^T)$ per block in terms of complex multiplications, which grows exponentially with T.

To achieve low complexity detection, we propose a single-user detector based on the MRC. For this detector, the l-th equalizer of the first user for the k-th subcarrier is given by

$$z_{l^{(1)},k} = \frac{\bar{h}_k^* c_{l^{(1)},k}^*}{\left|\bar{h}_k\right|^2 (T-1) + N_0} \tag{53}$$

for $l = 1, 2, \ldots, n/T$. Similar to (11) and (12), the estimate of the index of the spreading code for the first user can be obtained through

$$\hat{i}^{(1)} = \arg\max_{l^{(1)}} \left|\Delta_{l^{(1)}}\right|^2, \tag{54}$$

where $\Delta_{l^{(1)}} = \sum_{k=1}^{n} z_{l^{(1)},k} y_k$. Correspondingly, we have

$$\hat{s} = \arg\min_{s} \left| \sum_{k=1}^{n} z_{\hat{i},k} y_k - s \sum_{k=1}^{n} \frac{\left|\bar{h}_k\right|^2}{\left|\bar{h}_k\right|^2 (T-1) + N_0} \right|^2. \tag{55}$$

As seen from (54) and (55), the computational complexity per user is of order $\mathcal{O}(M + n/T)$.

In the uplink, we assume perfect synchronization or quasi-synchronization, in which the timing offsets between users are much smaller than the symbol duration. In such a scenario, the CP inserted for intersymbol interference prevention can also be used to contain timing offsets [30]. Moreover, the timing offset in the time domain is naturally transformed to the phase offset in the frequency domain at the receiver, which can be incorporated into the subcarrier channel estimation. Therefore, with perfect channel estimation the received signal at the base station is given by

$$y_k = \sum_{t=1}^{T} h_{t,k} s^{(t)} c_{i^{(t)},k} + w_k, \quad k = 1, \ldots, n, \tag{56}$$

where $h_{t,k}$ is the coefficient of the subchannel assigned to user t. Similar to the downlink of IM-MC-CDMA, both the single-user and multi-user detectors can be employed at the base station accordingly, which is omitted due to page limitations.

V. Simulation Results and Comparisons

In this section, the uncoded BER performance of IM/GIM-OFDM-SS and IM-MC-CDMA over Rayleigh fading channels is evaluated through Monte Carlo simulations. The BEP upper bounds and analytical BEP expressions are also examined. To show the superiority of the proposed IM-OFDM-SS scheme, it is compared with classical OFDM, OFDM-IM [9], DM-OFDM [22], CI-OFDM-IM [24], and OFDM-SS [28], while for multi-user systems, the proposed IM-MC-CDMA scheme is compared with the conventional MC-CDMA [28]. It is worth noting that the primary and the secondary constellations used by DM-OFDM are designed through constellation rotation. For simplicity, we will refer to "(CI-)OFDM-IM (n, n')" as the (CI-)OFDM-IM scheme in which n' out of n subcarriers are active, and "DM-OFDM (n, n')" as the DM-OFDM scheme in which n' out of n subcarriers are modulated by the primary constellation while the remaining subcarriers employ the secondary constellation.

A. IM-OFDM-SS Performance

In this subsection, the error performance of the IM-OFDM-SS scheme is assessed. To see the effects of different spreading codes, in Fig. 6, we present the BER curves of IM-OFDM-SS schemes with Zadoff-Chu and Walsh codes, where ML detectors, $n = 4$, and binary PSK (BPSK) are employed with $\sigma_e^2 = 0/0.01/0.05$. As seen from Fig. 6, the IM-OFDM-SS schemes with Zadoff-Chu codes outperform those with Walsh codes for $\sigma_e^2 = 0/0.01/0.05$ throughout the considered SNR region, which can be explained by the fact that IM-OFDM-SS schemes with Zadoff-Chu codes have larger minimum Euclidean distances between transmission vectors. In particular, we observe that without channel estimation errors, about 3 dB SNR gain at a BER value of 10^{-5} can be achieved by the scheme with Zadoff-Chu codes compared with the scheme using Walsh codes; however, both

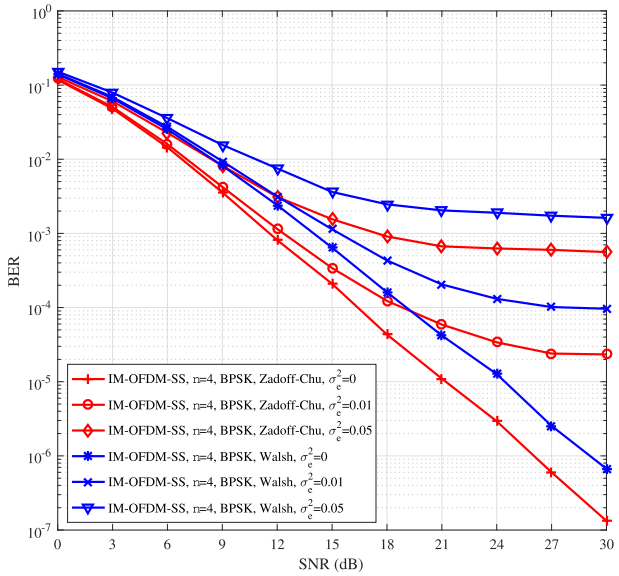

Fig. 6. Performance comparison between Zadoff-Chu and Walsh codes of IM-OFDM-SS with ML detectors (n=4, BPSK, $\sigma_e^2 = 0/0.01/0.05$).

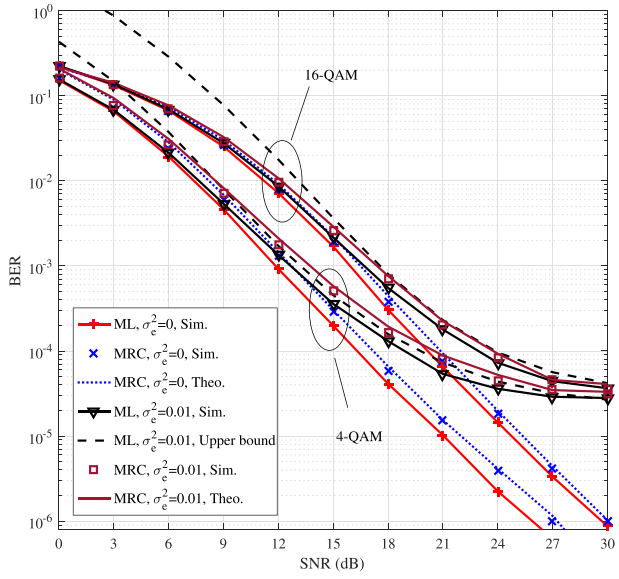

Fig. 7. Performance comparison between ML and MRC detectors of IM-OFDM-SS ($n = 4$, 4/16-QAM, $\sigma_e^2 = 0/0.01$).

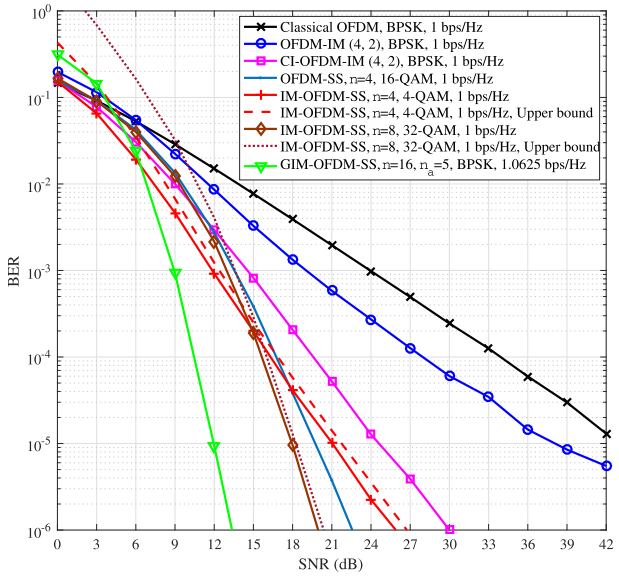

Fig. 8. Performance comparison among IM-OFDM-SS, GIM-OFDM-SS, classical OFDM, OFDM-IM, CI-OFDM-IM, and OFDM-SS at an SE of 1 bps/Hz, where ML detectors are used for all schemes.

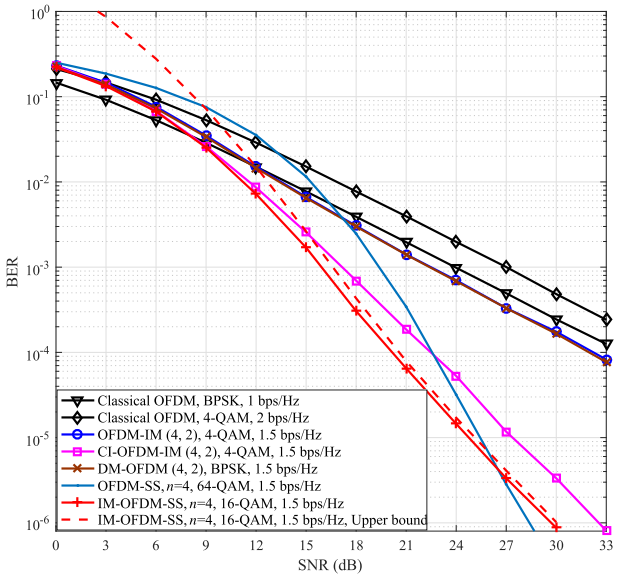

Fig. 9. Performance comparison among IM-OFDM-SS, classical OFDM, OFDM-IM, DM-OFDM, CI-OFDM-IM, and OFDM-SS at an SE level of 1.5 bps/Hz, where ML detectors are used for all schemes.

of them have the same diversity order of two. The channel estimation errors deteriorate the performance greatly and error floors are observed in the high SNR region due to the mismatched ML detectors. However, the error floors with Zadoff-Chu codes are lower than those with Walsh codes. In addition, Zadoff-Chu codes result in the lower peak to average power ratio [28]. Due to these advantages, Zadoff-Chu codes are adopted in the rest of computer simulations.

Fig. 7 presents the performance comparisons between ML and MRC detectors of IM-OFDM-SS, where $n = 4$ and 4/16-QAM are employed with $\sigma_e^2 = 0/0.01$. To verify the analyses given in Section III, in the figure, we also plot the BEP upper bounds (18) and the theoretical BEP curves (21) for ML and MRC detectors, respectively. For the clarity of presentation, the BEP upper bounds without channel estimation errors are provided in Figs. 8 and 9. It can be observed from Fig. 7 that MRC detectors exhibit near-ML performance with/without channel estimation errors. For $\sigma_e^2 = 0$, both detectors achieve the same diversity order and less than 1 dB SNR loss is incurred by the MRC detectors compared with the ML detectors. Besides, the BEP upper bounds become tight in the high SNR region and the approximate theoretical BEP curves agree with their simulation counterparts very well, no matter whether there exist channel estimation errors or not.

In Figs. 8–10, the BER performance of ML detection of IM-OFDM-SS without channel estimation errors is evaluated at various SEs. In Fig. 8, we compare the BER performance of

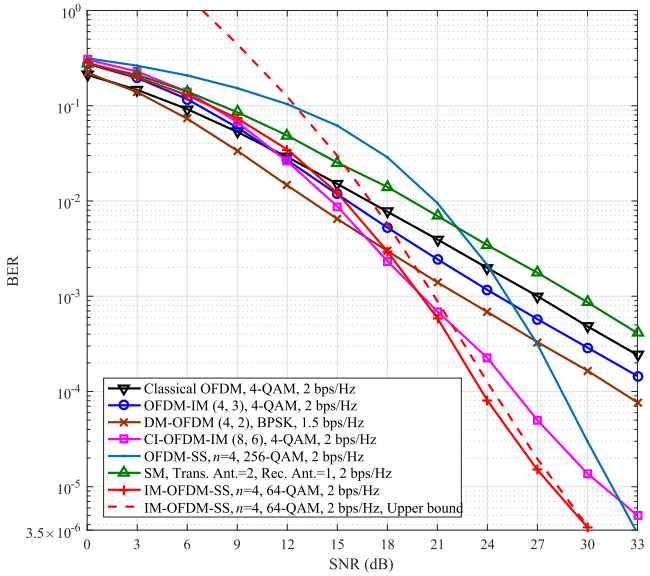

Fig. 10. Performance comparison among IM-OFDM-SS, classical OFDM, OFDM-IM, DM-OFDM, CI-OFDM-IM, OFDM-SS, and SM at an SE level of 1.5–2 bps/Hz, where ML detectors are used for all schemes.

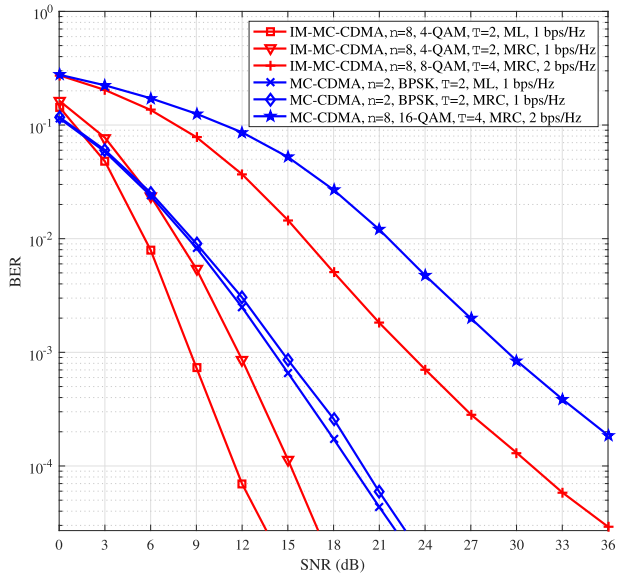

Fig. 11. Performance comparison between IM-MC-CDMA and conventional MC-CDMA in the downlink, where ML and MRC detectors are used.

IM-OFDM-SS with $n = 4$ (8) and 4-QAM (32-QAM), GIM-OFDM-SS with $n = 16$, $n_a = 5$, and BPSK, classical OFDM with BPSK, OFDM-IM with $(n, n') = (4, 2)$ and BPSK, CI-OFDM-IM with $(n, n') = (4, 2)$ and BPSK, and OFDM-SS with $n = 4$ and 16-QAM at an SE of 1 bps/Hz. All schemes employ ML detectors. From Fig. 8, we observe that the theoretical BEP upper bounds of IM-OFDM-SS agree with their computer simulation counterparts very well in the high SNR region. GIM-OFDM-SS, IM-OFDM-SS with $n = 8$, OFDM-SS, IM-OFDM-SS with $n = 4$, CI-OFDM-IM, OFDM-IM, and classical OFDM achieve diversity orders of 8, 4, 4, 2, 2, 1, and 1, respectively. The diversity order of IM/GIM-OFDM-SS increases with n and therefore, GIM-OFDM-SS with the highest diversity order performs the best in the SNR region of interest. Both IM-OFDM-SS schemes perform better than classical OFDM, OFDM-IM, and CI-OFDM-IM for all SNR values. More specifically, in spite of the same diversity order, IM-OFDM-SS with $n = 4$ and 4-QAM obtains approximately 3 dB SNR gain at a BER value of 10^{-5} over CI-OFDM-IM. Furthermore, IM-OFDM-SS with $n = 8$ and 32-QAM outperforms OFDM-SS throughout the considered SNR region and performs better than IM-OFDM-SS with $n = 4$ and 4-QAM at high SNR. Contrarily, because of the larger constellation size, IM-OFDM-SS with $n = 8$ and 32-QAM exhibits a worse BER than that with $n = 4$ and 4-QAM in the low SNR region.

Fig. 9 depicts the comparison results between IM-OFDM-SS with $n = 4$ and 16-QAM, classical OFDM with BPSK/4-QAM, OFDM-IM with $(n, n') = (4, 2)$ and 4-QAM, DM-OFDM with $(n, n') = (4, 2)$ and BPSK, CI-OFDM-IM with $(n, n') = (4, 2)$ and 4-QAM, and OFDM-SS with $n = 4$ and 64-QAM at an SE level of 1.5 bps/Hz. In DM-OFDM, two out of four subcarriers are modulated by the conventional BPSK, while the others employ $\pi/2$-rotated BPSK. ML detectors are used for all schemes and an SE of 1.5 bps/Hz is achieved except classical OFDM with BPSK (4-QAM) that has an SE of 1 bps/Hz (2 bps/Hz). Although it is not provided in the figure, the curve for classical OFDM with an SE of 1.5 bps/Hz can be predicted to be lying between those at 1 bps/Hz and 2 bps/Hz. As seen from the figure, IM-OFDM-SS performs the best among all schemes in the SNR region of interest. Although achieving a higher diversity order, OFDM-SS merely exhibits its superiority at high SNR due to its larger constellation size. DM-OFDM and OFDM-IM achieve a small SNR gain over classical OFDM; however all of them have the same diversity order of unity. DM-OFDM and OFDM-IM almost exhibit the same BER performance, which can be understood by the fact that the power saving with a factor of 50% stemming from the inactive subcarriers, corresponding to $10\log_{10}(2) \approx 3$ dB SNR gain provided by OFDM-IM, is counterbalanced by the modulation loss from BPSK to 4-QAM. On the other hand, IM-OFDM-SS achieves about 3 dB SNR gain over CI-OFDM-IM at a BER value of 10^{-5}.

The BER performance of IM-OFDM-SS with $n = 4$ and 64-QAM, classical OFDM with 4-QAM, OFDM-IM with $(n, n') = (4, 3)$ and 4-QAM, DM-OFDM with $(n, n') = (4, 2)$ and BPSK, CI-OFDM-IM with $(n, n') = (8, 6)$ and 4-QAM, OFDM-SS with $n = 4$ and 256-QAM, and plain SM with 2 transmit and 1 receive antennas at an SE level of 1.5–2 bps/Hz is compared in Fig. 10. ML detectors are used for all schemes and an SE of 2 bps/Hz is achieved except DM-OFDM, which has an SE of 1.5 bps/Hz. Similar to the observations in Figs. 8 and 9, IM-OFDM-SS and CI-OFDM-IM achieve a higher diversity order than classical OFDM, OFDM-IM, DM-OFDM, and SM. Approximately 3 dB SNR gain can be obtained at a BER value of 10^{-5} by IM-OFDM-SS compared with CI-OFDM-IM. Furthermore, in spite of a lower diversity order, IM-OFDM-SS performs better than OFDM-SS in the considered SNR region.

B. IM-MC-CDMA Performance

Fig. 11 shows the performance comparison between IM-MC-CDMA and conventional MC-CDMA in the downlink

TABLE I

COMPARISON OF DETECTION COMPLEXITY AMONG IM-OFDM-SS, CLASSICAL OFDM, OFDM-IM, AND OFDM-SS

	IM-OFDM-SS		Classical OFDM	OFDM-IM	OFDM-SS
	ML	MRC	ML		
1 bps/Hz	4 $(n=4, M=4)$	2	2 $(M=2)$	4 $(n=4, n'=2, M=2)$	4 $(n=4, M=16)$
	32 $(n=8, M=32)$	5			
1.5 bps/Hz	16 $(n=4, M=16)$	5	N.A.	16 $(n=4, n'=2, M=4)$	16 $(n=4, M=64)$
2 bps/Hz	64 $(n=4, M=64)$	17	4 $(M=4)$	64 $(n=4, n'=3, M=4)$	64 $(n=4, M=256)$

TABLE II

COMPARISON OF DETECTION COMPLEXITY BETWEEN IM-MC-CDMA AND MC-CDMA

	IM-MC-CDMA		MC-CDMA	
	ML	MRC	ML	MRC
1 bps/Hz	32 $(n=8, M=4, T=2)$	2	2 $(n=2, M=2, T=2)$	2
2 bps/Hz	8192 $(n=8, M=8, T=4)$	5	8192 $(n=8, M=16, T=4)$	8

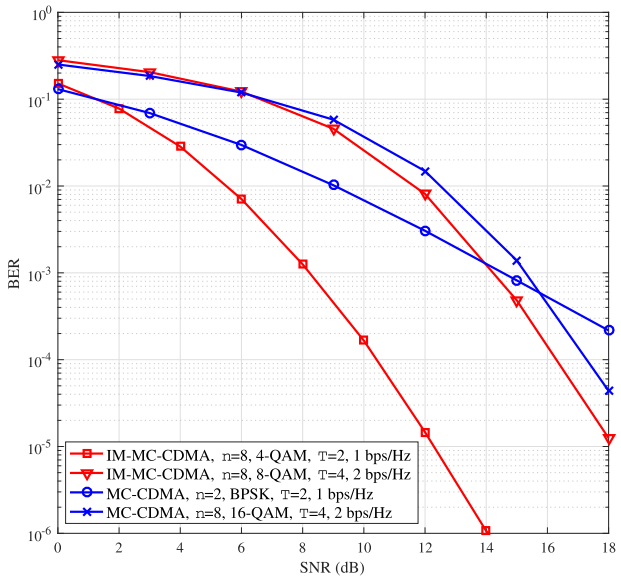

Fig. 12. Performance comparison between IM-MC-CDMA and conventional MC-CDMA in the uplink, where ML detectors are used.

at the overall SEs of 1 and 2 bps/Hz, where ML and MRC detectors are used for each scheme. For a fair comparison, the system parameters of IM-MC-CDMA and conventional MC-CDMA are set to achieve the same SE with the same number of users. It can be seen from Fig. 11 that for both IM-MC-CDMA and conventional MC-CDMA, the MRC detectors suffer from performance loss compared with ML detectors due to the multiple access interference. On the other hand, at both SEs, IM-MC-CDMA performs better than that of MC-CDMA in the SNR region of interest either for ML or MRC detection.

Fig. 12 gives the BER versus SNR curves for IM-MC-CDMA and conventional MC-CDMA in the uplink with ML detector at the base station. The system parameters are the same as those in Fig. 11. From Fig. 12, we observe that with the ML detector, IM-MC-CDMA outperforms conventional MC-CDMA at the SEs of 1 and 2 bps/Hz.

C. Complexity Comparison

In this subsection, the detection complexities of IM-OFDM-SS and IM-MC-CDMA are compared with those of other competitive schemes. For the single-user scenario, Table I lists the average number of metric calculations per subcarrier resulting by the ML and MRC detectors of IM-OFDM-SS, and ML detectors of classical OFDM, OFDM-IM, and OFDM-SS, which are calculated as M, $1+M/n$, M, $M^{n'}2^{\lfloor \log_2(C(n,n')) \rfloor}/n$, and M/n, respectively. For the downlink/uplink multi-user communications, Table II presents the average number of metric calculations per subcarrier resulting by ML and MRC detectors of IM-MC-CDMA and those detectors of MC-CDMA, which are calculated as $(Mn/T)^T/n$, $1+TM/n$, M^T/n, and TM/n, respectively. For a fair comparison, we select appropriate parameters for each scheme to obtain the same SEs. As shown in Tables I and II, our proposed IM-OFDM-SS and IM-MC-CDMA schemes achieve comparable detection complexities to other competitors.

VI. CONCLUSION

In this paper, we have proposed IM-OFDM-SS, in which the techniques of SS and IM are combined based on the framework of OFDM to improve the performance of existing OFDM, OFDM-IM, and OFDM-SS schemes. IM-OFDM-SS spreads an M-ary modulated symbol over several subcarriers by a spreading code and utilizes the index of the selected spreading code to convey additional bits. A low-complexity MRC-based detector has been designed for IM-OFDM-SS. An upper bound and an approximate mathematical expression for the BEP have been derived, taking into account the channel estimation errors. Subsequently, two extensions of IM-OFDM-SS have been proposed, including GIM-OFDM-SS in which

$$P_{sb}\left(f_{1,j}^{I}\right)=\frac{1}{\pi}\int_{0}^{\pi/2}\left[\int_{0}^{\infty}\exp\left(-\frac{\gamma_k\left(-\rho d_{s,j}^{I}\right)^2}{\sin^2\phi}\right)f_{\gamma_k}\left(\gamma_k\right)d\gamma_k\right]^n d\phi=\frac{1}{\pi}\int_{0}^{\pi/2}\left(\frac{\sin^2\phi}{\bar{\gamma}\left(-\rho d_{s,j}^{I}\right)^2+\sin^2\phi}\right)^n d\phi$$
$$=\left(\frac{1-\mu_c}{2}\right)^n\sum_{k=0}^{n-1}C\left(n-1+k,k\right)\left(\frac{1+\mu_c}{2}\right)^k \tag{63}$$

multiple spreading codes are activated for one user to improve the SE, and IM-MC-CDMA in which each user/base station is equipped with the IM-OFDM-SS transceiver. Finally, the BER performance of IM/GIM-OFDM-SS and IM-MC-CDMA has been simulated extensively, whose results show that IM/GIM-OFDM-SS significantly outperforms classical OFDM as well as the existing OFDM-IM and OFDM-SS schemes, and IM-MC-CDMA performs better than conventional MC-CDMA at the same SEs for either multi-user or single-user detection.

We remark that in the presence of asynchronous users, the performance of IM-MC-CDMA would be deteriorated as in the conventional MC-CDMA. The performance analysis for this case will be considered as our future work.

Appendix
Proof of (39)

The conditional error probability for bit $f_{1,j}^{I}$, $P_{sb}(f_{1,j}^{I}|\{\gamma\}_{k=1}^{n})$, is given by

$$P_{sb}\left(f_{1,j}^{I}|\{\gamma_k\}_{k=1}^{n}\right)=Q\left(\sqrt{2\gamma_{total}}\left(-\rho d_{s,j}^{I}\right)\right), \tag{57}$$

where $\gamma_{total}=\sum_{k=1}^{n}\gamma_k$ is the total instantaneous conditional SNR with

$$\gamma_k=\frac{|\bar{h}_k|^2}{(1-\rho)\left(d_{s,j}^{I}\right)^2+N_0}. \tag{58}$$

To obtain the average error probability, $P_{sb}(f_{1,j}^{I})$, (57) has to be statistically averaged over the joint PDF of $\{\gamma_k\}_{k=1}^{n}$. Since random variables $\{\gamma_k\}_{k=1}^{n}$ are assumed to be independent, we have

$$P_{sb}\left(f_{1,j}^{I}\right)=\underbrace{\int_{0}^{\infty}\cdots\int_{0}^{\infty}}_{n-fold}P_{sb}(f_{1,j}^{I}|\{\gamma_k\}_{k=1}^{n})\times\prod_{k=1}^{n}f_{\gamma_k}\left(\gamma_k\right)d\gamma_1\cdots d\gamma_n, \tag{59}$$

where $f_{\gamma_k}(\gamma_k)=\exp(-\gamma_k/\bar{\gamma})/\bar{\gamma}$ is the PDF of γ_k with $\bar{\gamma}=1/[\rho((1-\rho)(d_{s,j}^{I})^2+N_0)]$.

If $-\rho d_{s,j}^{I}\geq 0$, by using the alternative representation of Gaussian Q-function

$$Q\left(x\right)=\frac{1}{\pi}\int_{0}^{\pi/2}\exp\left(-\frac{x^2}{2\sin^2\phi}\right)d\phi,\quad x\geq 0, \tag{60}$$

(57) can be expressed as

$$P_{sb}\left(f_{1,j}^{I}|\{\gamma_k\}_{k=1}^{n}\right)=\frac{1}{\pi}\int_{0}^{\pi/2}\exp\left(-\frac{\gamma_{total}\left(-\rho d_{s,j}^{I}\right)^2}{\sin^2\phi}\right)d\phi$$
$$=\frac{1}{\pi}\int_{0}^{\pi/2}\prod_{k=1}^{n}\exp\left(-\frac{\gamma_k\left(-\rho d_{s,j}^{I}\right)^2}{\sin^2\phi}\right)d\phi. \tag{61}$$

Substituting (61) into (59) results in

$$P_{sb}\left(f_{1,j}^{I}\right)=\underbrace{\int_{0}^{\infty}\cdots\int_{0}^{\infty}}_{n-fold}\frac{1}{\pi}\int_{0}^{\pi/2}\prod_{k=1}^{n}\exp\left(-\frac{\gamma_k\left(-\rho d_{s,j}^{I}\right)^2}{\sin^2\phi}\right)\times f_{\gamma_k}\left(\gamma_k\right)d\phi d\gamma_1\cdots d\gamma_n. \tag{62}$$

Interchanging the order of integration and grouping the terms of index k, we can formulate (62) as (63), shown at the top of this page, where $\mu_c=\sqrt{\frac{\bar{\gamma}\left(-\rho d_{s,j}^{I}\right)^2}{1+\bar{\gamma}\left(-\rho d_{s,j}^{I}\right)^2}}$ and in the derivation of the last equality, we have considered [40, eq. (5A.4b)].

If $-\rho d_{s,j}^{I}<0$, using the equation $Q(x)=1-Q(-x)$, we obtain

$$P_{sb}\left(f_{1,j}^{I}\right)=1-\left(\frac{1-\mu_c}{2}\right)^n\sum_{k=0}^{n-1}C(n-1+k,k)\left(\frac{1+\mu_c}{2}\right)^k. \tag{64}$$

Therefore, putting (63) and (64) together yields (39), completing the proof.

References

[1] R. W. Chang, "Synthesis of band-limited orthogonal signals for multichannel data transmission," *Bell Labs Tech. J.*, vol. 45, no. 45, pp. 1775–1796, Dec. 1966.

[2] S. B. Weinstein and P. M. Ebert, "Data transmission by frequency-division multiplexing using the discrete Fourier transform," *IEEE Trans. Commun.*, vol. COM-19, no. 5, pp. 628–634, Oct. 1971.

[3] *Digital Video Broadcasting (DVB); Framing Structure, Channel Coding and Modulation for Digital Terrestrial Television*, ETSI Standard EN 300 744 (V1.5.1), Nov. 2004.

[4] *LAN/MAN Specific Requirements—Part 2: Wireless MAC and PHY Specifications for High Speed Physical Layer in the 5 GHz Band*, IEEE Standard 802.11, May 1999.

[5] E. Basar, "Index modulation techniques for 5G wireless networks," *IEEE Commun. Mag.*, vol. 54, no. 7, pp. 168–175, Jul. 2016.

[6] P. Yang, M. Di Renzo, Y. Xiao, S. Li, and L. Hanzo, "Design guidelines for spatial modulation," *IEEE Commun. Surveys Tuts.*, vol. 17, no. 1, pp. 6–26, 1st Quart., 2015.

[7] R. Abualhiga and H. Haas, "Subcarrier-index modulation OFDM," in *Proc. IEEE 20th Int. Symp. Pers., Indoor Mobile Radio Commun. (PIMRC)*, Tokyo, Japan, Sep. 2009, pp. 177–181.

[8] D. Tsonev, S. Sinanovic, and H. Haas, "Enhanced subcarrier index modulation (SIM) OFDM," in *Proc. IEEE Global Commun. Conf. (GLOBECOM) Workshops*, Houston, TX, USA, Dec. 2011, pp. 728–732.
[9] E. Basar, U. Aygolu, E. Panayirci, and H. V. Poor, "Orthogonal frequency division multiplexing with index modulation," *IEEE Trans. Signal Process.*, vol. 61, no. 22, pp. 5536–5549, Nov. 2013.
[10] N. Ishikawa, S. Sugiura, and L. Hanzo, "Subcarrier-index modulation aided OFDM—Will it work?" *IEEE Access*, vol. 4, pp. 2580–2593, Jun. 2016.
[11] M. Wen, X. Cheng, M. Ma, B. Jiao, and H. V. Poor, "On the achievable rate of OFDM with index modulation," *IEEE Trans. Signal Process.*, vol. 64, no. 8, pp. 1919–1932, Apr. 2016.
[12] Q. Ma, P. Yang, Y. Xiao, H. Bai, and S. Li, "Error probability analysis of OFDM-IM with carrier frequency offset," *IEEE Commun. Lett.*, vol. 20, no. 12, pp. 2434–2437, Dec. 2016.
[13] J. Crawford and Y. Ko, "Low complexity greedy detection method with generalized multicarrier index keying OFDM," in *Proc. IEEE 26th Annu. Int. Symp. Pers., Indoor, Mobile Radio Commun.*, Hong Kong, Aug. 2015, pp. 688–693.
[14] Y. Ko, "A tight upper bound on bit error rate of joint OFDM and multicarrier index keying," *IEEE Commun. Lett.*, vol. 18, no. 10, pp. 1763–1766, Oct. 2014.
[15] A. I. Siddiq, "Effect of subcarrier activation ratio on the performance of OFDM-IM over Rayleigh fading channel," *IEEE Commun. Lett.*, vol. 21, no. 6, pp. 1293–1296, Jun. 2017.
[16] R. Fan, Y. J. Yu, and Y. L. Guan, "Generalization of orthogonal frequency division multiplexing with index modulation," *IEEE Trans. Wireless Commun.*, vol. 14, no. 10, pp. 5350–5359, Oct. 2015.
[17] H. Zhang, L.-L. Yang, and L. Hanzo, "Compressed sensing improves the performance of subcarrier index-modulation assisted OFDM," *IEEE Access*, vol. 4, pp. 7859–7873, Oct. 2016.
[18] E. Basar, "On multiple-input multiple-output OFDM with index modulation for next generation wireless networks," *IEEE Trans. Signal Process.*, vol. 64, no. 15, pp. 3868–3878, Aug. 2016.
[19] B. Zheng, M. Wen, E. Basar, and F. Chen, "Multiple-input multiple-output OFDM with index modulation: Low-complexity detector design," *IEEE Trans. Signal Process.*, vol. 65, no. 11, pp. 2758–2772, Jun. 2017.
[20] T. Datta, H. S. Eshwaraiah, and A. Chockalingam, "Generalized space and frequency index modulation," *IEEE Trans. Veh. Tech.*, vol. 65, no. 7, pp. 4911–4924, Jul. 2016.
[21] B. Chakrapani, T. L. Narasimhan, and A. Chockalingam, "Generalized space-frequency index modulation: Low-complexity encoding and detection," in *Proc. IEEE Globecom Workshops (GC Wkshps)*, San Diego, CA, USA, Dec. 2015, pp. 1–6.
[22] T. Mao, Z. Wang, Q. Wang, S. Chen, and L. Hanzo, "Dual-mode index modulation aided OFDM," *IEEE Access*, vol. 5, pp. 50–60, Feb. 2017.
[23] Y. Xiao, S. Wang, L. Dan, X. Lei, P. Yang, and W. Xiang, "OFDM with interleaved subcarrier-index modulation," *IEEE Commun. Lett.*, vol. 18, no. 8, pp. 1447–1450, Aug. 2014.
[24] E. Başar, "OFDM with index modulation using coordinate interleaving," *IEEE Wireless Commun. Lett.*, vol. 4, no. 4, pp. 381–384, Aug. 2015.
[25] J. Choi, "Coded OFDM-IM with transmit diversity," *IEEE Trans. Commun.*, vol. 65, no. 7, pp. 3164–3171, Jul. 2017.
[26] L. Wang, Z. Chen, Z. Gong, and M. Wu, "Space-frequency coded index modulation with linear-complexity maximum likelihood receiver in the MIMO-OFDM system," *IEEE Signal Process. Lett.*, vol. 23, no. 10, pp. 1439–1443, Oct. 2016.
[27] J. Crawford, E. Chatziantoniou, and Y. Ko, "On the SEP analysis of OFDM index modulation with hybrid low complexity greedy detection and diversity reception," *IEEE Trans. Veh. Tech.*, vol. 66, no. 9, pp. 8103–8118, Sep. 2017.
[28] L.-L. Yang, *Multicarrier Communications*. Hoboken, NJ, USA: Wiley, 2009.
[29] A. Chouly, A. Brajal, and S. Jourdan, "Orthogonal multicarrier techniques applied to direct sequence spread spectrum CDMA systems," in *Proc. GLOBECOM*, Houston, TX, USA, Nov. 1993, pp. 1723–1728.
[30] A. C. McCormick and E. A. Al-Susa, "Multicarrier CDMA for future generation mobile communication," *Electron. Commun. Eng. J.*, vol. 14, no. 2, pp. 52–60, Apr. 2002.
[31] J. Zhang, L.-L. Yang, L. Hanzo, and H. Gharavi, "Advances in cooperative single-carrier FDMA communications: Beyond LTE-advanced," *IEEE Commun. Surveys Tuts.*, vol. 17, no. 2, pp. 730–756, May 2015.
[32] G. Kaddoum, M. F. A. Ahmed, and Y. Nijsure, "Code index modulation: A high data rate and energy efficient communication system," *IEEE Commun. Lett.*, vol. 19, no. 2, pp. 175–178, Feb. 2015.
[33] G. Kaddoum, Y. Nijsure, and H. Tran, "Generalized code index modulation technique for high data rate communication systems," *IEEE Trans. Veh. Technol.*, vol. 65, no. 9, pp. 7000–7009, Sep. 2016.
[34] G. Kaddoum and E. Soujeri, "On the comparison between code-index modulation and spatial modulation techniques," in *Proc. Int. Conf. Inf. Commun. Technol. Res. (ICTRC)*, Abu Dhabi, United Arab Emirates, May 2015, pp. 24–27.
[35] W. Xu and L. Wang, "CIM-DCSK: A differential chaos shift keying scheme with code-index modulation," in *Proc. Int. Symp. Commun. Inf. Technol. (ISCIT)*, Qingdao, China, Sep. 2016, pp. 100–104.
[36] D. C. Chu, "Polyphase codes with good periodic correlation properties," *IEEE Trans. Inf. Theory*, vol. IT-18, no. 4, pp. 531–532, Jul. 1972.
[37] P. K. Frenger and N. A. B. Svensson, "Parallel combinatory OFDM signaling," *IEEE Trans. Commun.*, vol. 47, no. 4, pp. 558–567, Apr. 1999.
[38] V. Tarokh, A. Naguib, N. Seshadri, and A. R. Calderbank, "Space-time codes for high data rate wireless communication: Performance criteria in the presence of channel estimation errors, mobility, and multiple paths," *IEEE Trans. Commun.*, vol. 47, no. 2, pp. 199–207, Feb. 1999.
[39] L. Zhang, L. Song, M. Ma, and B. Jiao, "On the minimum differential feedback for time-correlated MIMO Rayleigh block-fading channels," *IEEE Trans. Commun.*, vol. 60, no. 2, pp. 411–420, Feb. 2012.
[40] M. K. Simon and M.-S. Alouini, *Digital Communication Over Fading Channels*, 2nd ed. New York, NY, USA: Wiley, 2005.
[41] P. K. Vitthaladevuni and M. S. Alouini, "A closed-form expression for the exact BER of generalized PAM and QAM constellations," *IEEE Trans. Commun.*, vol. 52, no. 5, pp. 698–700, May 2004.
[42] M. Wen, X. Cheng, M. Wang, B. Ai, and B. Jiao, "Error probability analysis of interleaved SC-FDMA systems over Nakagami-*m* frequency selective fading channels," *IEEE Trans. Veh. Tech.*, vol. 62, no. 2, pp. 748–761, Feb. 2013.

Qiang Li received the B.S. degree from the Inner Mongolia University of Science and Technology, Baotou, China, in 2013, and the M.S. degree from the Nanjing University of Aeronautics and Astronautics, Nanjing, China, in 2016. He is currently pursuing the Ph.D. degree with the South China University of Technology, Guangzhou, China. His current research interests include MIMO systems, index modulation, and OFDM.

Miaowen Wen (M'14) received the B.S. degree from Beijing Jiaotong University, Beijing, China, in 2009, and the Ph.D. degree from Peking University, Beijing, in 2014. From 2012 to 2013, he was a Visiting Student Research Collaborator with Princeton University, Princeton, NJ, USA. He is currently an Associate Professor with the South China University of Technology, Guangzhou, China. He has authored a book and over 80 papers in refereed journals and conference proceedings. His research interests include index modulation, non-orthogonal multiple access, physical layer security, and molecular communications.

He was a recipient of the Excellent Doctoral Dissertation Award from Peking University and the Best Paper Awards from the IEEE International Conference on Intelligent Transportation Systems Telecommunications in 2012, the IEEE International Conference on Intelligent Transportation Systems in 2014, and the IEEE International Conference on Computing, Networking and Communications in 2016. He was an Exemplary Reviewer of the IEEE COMMUNICATIONS LETTERS in 2017. He currently serves as an Associate Editor for the IEEE ACCESS and is on the Editorial Board of the *EURASIP Journal on Wireless Communications and Networking*, the *ETRI Journal*, and the *Physical Communication* (Elsevier).

Ertugrul Basar (S'09–M'13–SM'16) received the B.S. degree (Hons.) from Istanbul University, Turkey, in 2007, and the M.S. and Ph.D. degrees from Istanbul Technical University in 2009 and 2013, respectively. He was with the Department of Electrical Engineering, Princeton University, Princeton, NJ, USA, from 2011 to 2012. He was an Assistant Professor with Istanbul Technical University from 2014 to 2017, where he is currently an Associate Professor of electronics and communication engineering. He is an inventor of two pending patents on index modulation schemes. His research interests include MIMO systems, index modulation, cooperative communications, OFDM, and visible light communications.

Recent recognition of his research includes the Turkish Academy of Sciences Outstanding Young Scientist Award in 2017, the first-ever IEEE Turkey Research Encouragement Award in 2017, and the Istanbul Technical University Best Ph.D. Thesis Award in 2014. He was also a recipient of four best paper awards, including one from the IEEE International Conference on Communications in 2016. He has served as a TPC member for several IEEE conferences. He is a regular reviewer for various IEEE journals. He currently serves as an Associate Editor for the IEEE COMMUNICATIONS LETTERS and the IEEE ACCESS, and as an Editor of the *Physical Communication* (Elsevier).

Fangjiong Chen (M'06) received the B.S. degree in electronics and information technology from Zhejiang University, Hangzhou, China, in 1997, and the Ph.D. degree in communication and information engineering from the South China University of Technology, Guangzhou, China, in 2002. He was with the School of Electronics and Information Engineering, South China University of Technology. From 2002 to 2005, he was a Lecturer, and from 2005 to 2011, he was an Associate Professor with the South China University of Technology.

He is currently a full-time Professor with the School of Electronics and Information Engineering, South China University of Technology. He is the Director of the Department of Underwater Detection and Imaging, Mobile Ultrasonic Detection National Research Center of Engineering Technology. His research interests include signal detection and estimation, array signal processing, and wireless communication.

Professor Chen received the National Science Fund for Outstanding Young Scientists in 2013. He was elected to the New Century Excellent Talent Program of MOE, China, in 2012.